Available online at www.sciencedirect.com

ScienceDirect

Energy Procedia 142 (2017) 1468–1473

Energy Procedia

www.elsevier.com/locate/procedia

9th International Conference on Applied Energy, ICAE2017, 21-24 August 2017, Cardiff, UK

Zero-dimensional dynamic modeling of PEM electrolyzers

Paolo Colbertaldo[a]*, Sonia Laura Gómez Aláez[a], Stefano Campanari[a]

[a] *Department of Energy, Politecnico di Milano, Via Lambruschini 4A, 20156 Milano, Italy*

Abstract

The transition to a low-carbon system foresees the introduction of hydrogen as a clean energy vector. Electrolyzers play a key role in its production from renewable energy, and PEM technology seems the most promising alternative thanks to efficiency, flexibility and compactness. Modeling the device dynamic behavior allows investigating its combination with renewable electricity sources. A dynamic 0D model is developed using *Aspen Custom Modeler*, including a detailed description of the various phenomena involved in the electrochemical process. General formulations are implemented and multiple options for correlations are present, when available. The model is validated against available literature data, showing an appropriate reconstruction of the cell behavior. Unsteady behavior is studied and the role of thermal capacity is shown, under a test-case with a simple operating input profile.

Peer-review under responsibility of the scientific committee of the 9th International Conference on Applied Energy.

Keywords: electrolysis; modeling; dynamic; PEM.

1. Introduction

The development of a 'hydrogen economy' is considered a fundamental pathway for the transition to a low-carbon energy system. Within it, Power-to-Gas (P2G) is expected to play a key role, as a storage technology able to exploit excess electricity from renewables to produce clean fuels. The core element of a P2G system is the electrolyzer, whose dynamic behavior needs to be studied to assess the performance of the overall system when fed by intermittent sources. Among the available technologies, polymer electrolyte membrane (PEM) electrolyzers seem to surpass alkaline ones in terms of efficiency and compactness, while solid-oxide devices have not yet reached a commercial readiness level.

In this work, a zero-dimensional (0D) approach is applied to the development of a dynamic model of a PEM electrolyzer, and implemented in *Aspen Custom Modeler*. After a validation against literature data, simulations are

* Corresponding author. Tel.: +39-02-2399-3842
E-mail address: paolo.colbertaldo@polimi.it

1876-6102
Peer-review under responsibility of the scientific committee of the 9th International Conference on Applied Energy.
10.1016/j.egypro.2017.12.594

carried out to evaluate the performance of the electrolyzer under different conditions. The aim is to offer a simple, yet complete, description of the physical phenomena involved, including flexible selection of formulations or correlations for the estimation of parameters. The obtained versatile model will allow future integration into P2G systems analysis.

2. Model description

In a PEM electrolyzer, an electric current drives the decomposition of water, which is fed to the anode, into hydrogen and oxygen. The occurring reactions are:

$$\text{anode} \quad H_2O \rightarrow 2H^+ + 1/2\ O_2 + 2e^-$$

$$\text{cathode} \quad 2H^+ + 2e^- \rightarrow H_2$$

The electrolyte that separates the electrodes is a polymeric membrane (typically Nafion®), through which the charge carrier (H^+) moves from anode to cathode, where hydrogen is produced. These membranes offer high proton conductivity and low gas crossover, while the low thickness and the high current densities (up to 2 A cm^{-2}) allow for a compact design [1]. The electrodes are usually metals (typically Ti) with catalysts based on Pt, Ir or Ru. The operating pressure ranges from 1 to 200 bar, while temperature is maintained between 20 and 80 °C. The specific electricity consumption is about 5 kWh/Nm^3_{H2}.

2.1. Voltage

The electrolyzer is composed of many cells connected in series to form a stack, thus allowing to operate with a higher voltage at the external connections, while keeping the same current flowing across the cells. Focusing on a single cell, the required voltage is equal to the sum of the ideal voltage ('id') and the overpotentials, due to the losses:

$$V_{cell}(T,p,I_{cell}) = V_{id}(T,p) + \sum \Delta V_{cell}(T,p,I_{cell}) = V_{id} + \Delta V_{act} + \Delta V_{ohm} + \Delta V_{diff} + \Delta V_{par}$$

The ideal voltage depends on the reaction electrochemistry and can be calculated from the Gibbs free energy variation ΔG° with a pressure correction:

$$V_{id} = \frac{\Delta G^{\circ}(T,p_{ref})}{nF} + \frac{RT}{nF} ln\left(\frac{p_{H_2}\ p_{O_2}^{0.5}}{a_{H_2O}}\right)$$

where n is the number of moles of electrons involved in the overall reaction, F is the Faraday constant (96485 C/mol), p_A is the partial pressure of component A and a_{H_2O} is the activity of water fed in liquid state.

The activation ('act') overpotential represents the extra voltage required to start the reactions, whose evolution is driven by kinetics. The charge transfer process between electrodes and electrolyte determines an excess charge close to the electrodes, generating a high electric field to be crossed by the charged ions. These losses are the most difficult to model, due to their dependence on the reaction, the catalyst, the reactant activities and the current density. The Tafel equation is implemented, which is a simplified formulation of the implicit Butler-Volmer equation [2]:

$$\Delta V_{act,X} = \frac{RT}{\alpha_X\ n\ F}\ ln\left(\frac{i_X}{i_{0,X}}\right)$$

where X is either anode or cathode, $i_{0,X}$ is the exchange current density, corresponding to the current density for the reversible semi-reaction, and α_X is the charge transfer coefficient, whose value varies between 0 and 1 ($\alpha_{an} = 0.5$ and $\alpha_{cat} = 0.5$ are used in the model, as suggested in literature [3]).

The ohmic ('ohm') overpotential is determined by the electric resistance of electrodes and membrane (Ohm's Law):

$$\Delta V_{ohm} = (R_{electrodes} + R_{mem}) i_{useful} A$$

Ideal anode and cathode electrodes offer low resistance to both electrons and protons (H^+ ions), while the membrane facilitates protons movement and avoids (as much as possible) the permeation of other components. Analytically:

$$R_{electrodes} = R_{anode} + R_{cathode} = \frac{t_{an}\ \rho_{an}}{A} + \frac{t_{cat}\ \rho_{cat}}{A}$$

$$R_{mem} = \frac{t_{mem}}{\sigma_{mem}\ A}$$

where t is the thickness, ρ_X is the electrical resistivity of each electrode and σ_{mem} is the proton conductivity of the membrane, for which models are presented in Table 1.

The diffusion ('diff') losses are due to mass transport limitations, determined by the concentration gradient between the bulk flow and the reaction sites on the membrane surface. They depend on the current, the reactant activity and the electrodes structure. The general analytical expression shows a Nernst-like dependence on the temperature and on the concentration in the bulk phase and in the reaction phase [1]. However, the overpotential can be modeled by defining a current limiting term i_L and considering only the anode side, whose contribution is the dominant one [2]:

$$\Delta V_{diff} = \frac{RT}{\alpha_{an}\, n\, F} \ln\left(\frac{i_L}{i_L - i_{an}}\right)$$

Experimental evidence has shown that the influence of this term is much smaller than the two previous contributions, and many authors consider it negligible [1][4]. It is included in the developed model, since its role could become significant at very high current densities; however, the high value (6 A/cm^2) assumed for i_L (as suggested in [2][5]) makes its contribution almost null in the assumed operating range (see Figure 1b).

Parasitic ('par') losses are usually modeled as a current variation rather than a voltage increase. They correspond to the presence of undesired short-circuit currents and crossover phenomena within the cell, which increase the electric consumption. The ratio of the useful current I_{useful} to the total current I_{stack} is called Faraday's efficiency η_F:

$$I_{stack}\, \eta_F = I_{useful} = i_{useful}\, A$$

The Faraday's efficiency is often assumed as a fixed value or even neglected, due to experimental analyses showing values close to 1. In this work, a value of 0.99 is assumed, according to literature [6].

Table 1. Models for the estimation of membrane proton conductivity.

Model	*Formula*
Kopitzke [7]	$\sigma_{mem} = 2.29 \exp\left(-\frac{7829}{RT}\right)$
Springer [8]	$\sigma_{mem} = (0.005139\lambda - 0.00326) \exp\left(1268\left(\frac{1}{303} - \frac{1}{T}\right)\right)$
Bernardi [5]	$\sigma_{mem} = \frac{F^2\, C^{H^+} D^{H^+}_{mem}}{RT}$

2.2. Material balance

The hydrogen production rate at the cathode depends on the electrochemical behavior of the cells. The associated consumption of water and production of oxygen are determined accordingly, by respecting the reaction stoichiometry:

$$n\, F\, \dot{N}_{H_2} = i_{useful}\, A\, N_{cells}$$

Although designed to allow only proton permeation, the membrane is not completely impermeable to water, which diffuses across it through three main effects (formulas refer to the transport from anode to cathode):

- electro-osmotic drag ('eo'), i.e. the transport of water molecules by hydrogen ions [3][9]:
$$F\, \dot{N}^{eo}_{H_2O} = n_d\, i_{useful}\, A\, N_{cells}$$
where the coefficient n_d can be assumed constant or dependent on membrane humidification [10]:
$$n_d = 0.0029\, \lambda^2 + 0.05\lambda - 3.4 \cdot 10^{-19}$$
- diffusivity-driven transport ('Diff'), due to the difference in concentration between anode and cathode [9]:
$$\dot{N}^{Diff}_{H_2O} = \frac{D_{H_2O,effective}\, \left(C_{H_2O,an} - C_{H_2O,cat}\right) A\, N_{cells}}{t_{mem}}$$
The effective diffusivity is determined from the temperature-dependent diffusivity [11] and the porosity ε [9]:
$$D_{H_2O,effective} = D_{H_2O}\, \varepsilon^{1.5} = 0.256\left(\frac{T}{273.15}\right)^{1.823} \varepsilon^{1.5}$$
- pressure-driven cross-flow ('p'), caused by the pressure difference at the two sides of the membrane [3]:
$$\dot{N}^{p}_{H_2O} = -\frac{K_{Darcy}\, \mathrm{A}\, \rho_{H_2O}\, (p_{cat} - p_{an})}{t_{mem}\, \mu_{H_2O}\, MM_{H_2O}}$$
where K_{Darcy} is the membrane permeability to water.

The material balance can be written considering the molar flow rates ($\dot{N}$, mol/s) of hydrogen, oxygen and water at both electrodes. The mass balance is developed without considering a storage term, whose implementation would have required detailed information about the channel geometry, which is outside the scope of this preliminary work. It is therefore expressed, on molar basis, as:

$$\dot{N}_{H_2,cat,out} = \dot{N}_{H_2,cat,in} + \dot{N}_{H_2,prod}$$
$$\dot{N}_{O_2,an,out} = \dot{N}_{O_2,an,in} + \dot{N}_{O_2,prod}$$
$$\dot{N}_{H_2O,an,out} = \dot{N}_{H_2O,an,in} - \dot{N}_{H_2O,cons} - \dot{N}^{eo}_{H_2O} - \dot{N}^{Diff}_{H_2O}$$
$$\dot{N}_{H_2O,cat,out} = \dot{N}_{H_2O,cat,in} + \dot{N}^{eo}_{H_2O} + \dot{N}^{Diff}_{H_2O}$$

2.3. Energy balance

Water splitting is a nonspontaneous endothermic reaction, therefore it requires energy to occur, which is fed to the system in the form of electric energy. The overall energy balance is:

$$C_{tot}\frac{dT}{dt} = \dot{H}_{in} - \dot{H}_{out} - \dot{Q}_{loss} + P_{el}$$

where cooling is indirectly accounted for as a temperature (and therefore enthalpy) variation of the flow between inlet and outlet. C_{tot} is the system total thermal capacity. The quantity $\dot{Q}_{loss}$ is the thermal power exchanged between the external wall of the stack case and ambient air. It can be either imposed (as null, as a constant or as a fixed fraction of the enthalpy variation across the cell) or evaluated using the complete heat transfer equation:

$$\dot{Q}_{loss} = UA\,(T_{wall,ext} - T_{amb})$$

where the global heat transfer coefficient U (W/m^{2}K) could be given by the manufacturer or estimated through correlations, involving convective and radiative contributions.

3. Simulations results and discussion

Due to their modularity, the size of the devices ranges widely, based on uses and system integration. In order to have a consistent set of data to check the validity of the developed model, operating values are mainly taken from [9][14]. Physical properties and parameters are summarized in Table 2. The Springer model (see Table 1) is used to determine the membrane conductivity, while the complete estimation of UA is performed in the unsteady simulations.

Table 2. List of parameters.

Parameter	*Value*	*Parameter*	*Value*
Exchange current density anode [3][12]	$i_{0,an} = 1\cdot 10^{-10}\frac{A}{cm^2}$	Membrane thickness [9]	$t_{mem} = 127\ \mu m$
Exchange current density cathode [3][12]	$i_{0,cat} = 1\cdot 10^{-3}\frac{A}{cm^2}$	Membrane porosity [9]	$\varepsilon = 0.3$
Active cell area [9]	$A_{cell} = 160\ cm^2$	Membrane humidification [4]	$\lambda = 22$
Number of cells [9]	$N_{cells} = 12$	Membrane proton diffusivity [12]	$D^{H^+}_{mem} = 1.28\cdot 10^{-6}\frac{cm^2}{s}$
Electrode resistivity [1][13]	$\rho_{el} = 7.5\ m\Omega\ cm$	Membrane proton concentration [12]	$C^{H^+}_{mem} = 1\frac{kmol}{m^3}$
Electrode thickness [1][13]	$t_{el} = 1.3\ mm$	Inlet volumetric flow rate [9]	$\dot{V}_{H_2O} = 5.5\frac{l}{min}$

3.1. Steady-state behavior

The polarization curve of the electrolyzer cell at different operating conditions is shown in Figure 1a. At small values of the current density (up to 0.5 A/m^2), the cell potential only shows dependence with the pressure (mainly due to a different ideal voltage). At higher current densities, the effect of temperature becomes significant. In general, the required potential increases with higher pressures and with lower temperatures.

In Figure 1b, the role of the different overpotentials is highlighted. When the current density increases, the ideal potential decreases slightly due to the correspondent increment of the cell operating temperature. On the contrary, ΔV_{ohm} and the other overpotentials grow significantly, so that the overall effect is an increase of the real potential. The voltage reaches 2.51 V at 2 A/cm^2, while the ideal potential is about 1.21 V. The diffusion overpotential yields a negligible contribute, due to the high value assumed for the limiting current.

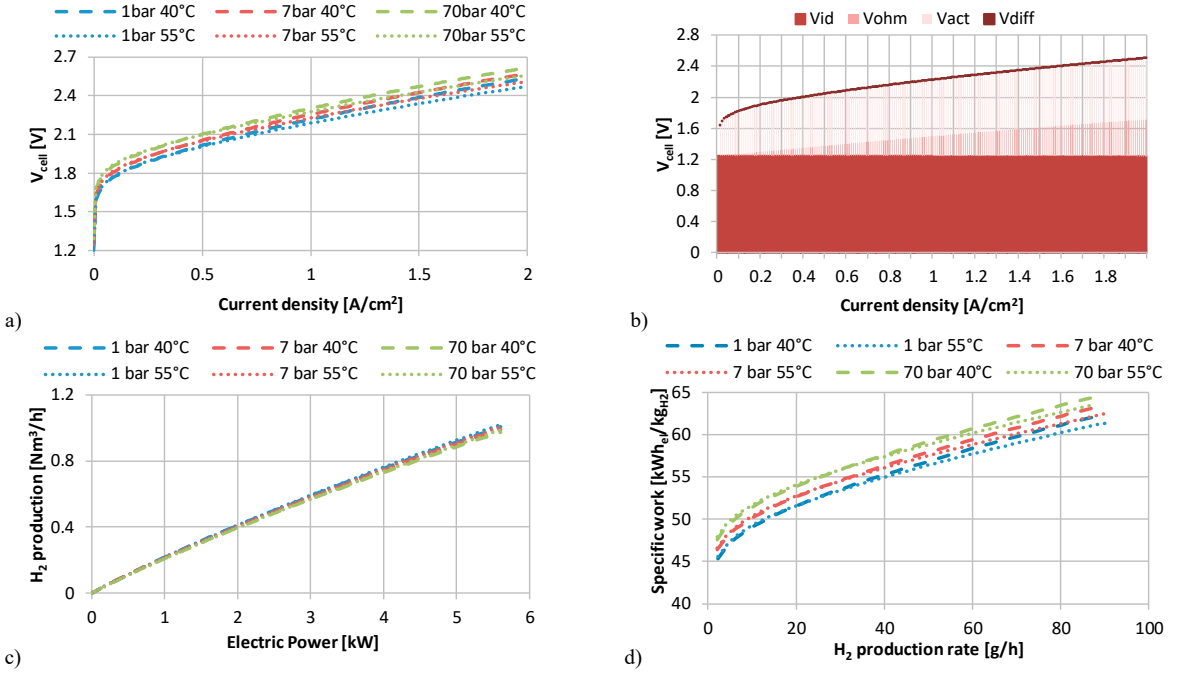

Figure 1. Steady state results: a) polarization curve; b) influence of overpotentials; c) hydrogen production rate; d) specific electric consumption.

Given the electric power input, a higher operating temperature shifts down the polarization curve, thus lowering the required voltage and allowing for greater current, leading to a higher hydrogen production due to its linear dependence (see Figure 1c). At fixed temperature, the same effect can be obtained by lowering the operating pressure.

The performance of the electrolyzer is commonly evaluated with the specific electric consumption (kWh/kg$_{H2}$), plotted in Figure 1d versus the hydrogen production rate. The specific consumption increases with the H_2 production rate, owing to the higher overpotentials brought about by an operation at increasingly high electric power input (see Figure 1c) and higher current density. Moreover, the effect of diverse operating conditions is depicted: higher temperature and lower pressure determine smaller overpotentials in the polarization curve and thus a smaller specific energy consumption, up to 4% reduction from 70 to 1 bar. The obtained profiles and the considerations made are coherent with the results presented in [9], whose datasets were also used as a reference in Table 2. In terms of efficiency (hydrogen LHV energy content over the electric power input), values exceed 50% in all simulated cases, with higher figures at low electric power input (e.g. up to 72%), thanks to the lower overpotentials.

3.2. Dynamics

The developed model can be applied to study the dynamic thermal behavior of the stack through the unsteady energy balance, for instance allowing to analyze the response time of the system to input variations. Here, an example is considered where the stack is fed with a variable electric power input, with a profile that includes a start up and a shut down (see Figure 2), simulating the temperature evolution. The temperature dynamics is driven by the thermal capacity C_{tot}, for which a reference value of 0.055 W/K is selected (actual values depend on detailed stack data) and compared with two cases overestimated by 50% and 100%. As expected, it is shown that the variation does not affect the steady-

state solution, but it influences the time required to reach a stable condition. Smaller values of the thermal capacity allow a faster response of the temperature to the variation of the electric power input.

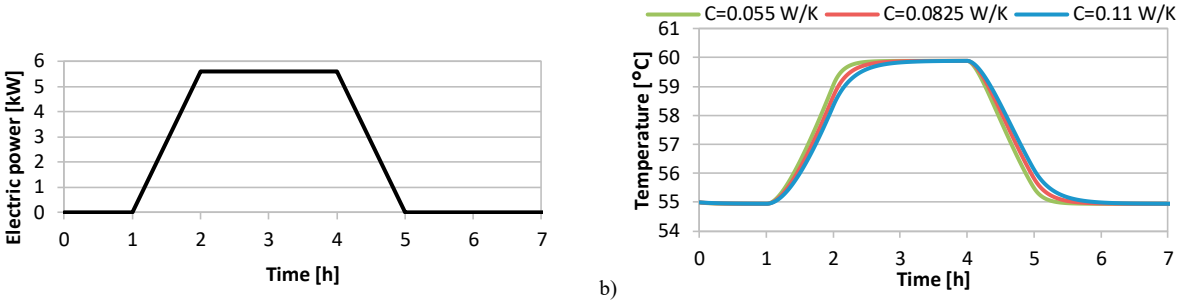

a) b)

Figure 2. Dynamics simulations: a) profile of electric power input; b) profiles of operating stack temperature with different thermal capacities.

4. Conclusions

A complete 0D model of a PEM electrolyzer has been developed, capable to simulate the overall performance considering the various phenomena that take place in a stack. The properties of the components are either directly specified as parameters or evaluated from correlations, for which multiple formulations are included.

Simulations based on literature data have shown a consistent reconstruction of the device behavior, and an unsteady study has been performed to study the thermal dynamics.

Further work will address the dynamic response to more fluctuating input profiles, while the description of the internal geometry will allow a more detailed reconstruction of the mass dynamics. Moreover, the integration within P2G systems will lead to an analysis of the dynamic capabilities of this energy conversion and storage technology.

References

[1] M. Carmo, D. L. Fritz, J. Mergel, and D. Stolten, “A comprehensive review on PEM water electrolysis,” *Int. J. Hydrogen Energy*, vol. 38, no. 12, pp. 4901–4934, 2013

[2] R. García-Valverde, N. Espinosa, and A. Urbina, “Simple PEM water electrolyser model and experimental validation,” *Int. J. Hydrogen Energy*, vol. 37, no. 2, pp. 1927–1938, 2012.

[3] Z. Abdin, C. J. Webb, and E. M. Gray, “Modelling and simulation of a proton exchange membrane (PEM) electrolyser cell,” *Int. J. Hydrogen Energy*, vol. 40, no. 39, pp. 13243–13257, 2015

[4] M. E. Lebbal and S. Lecœuche, “Identification and monitoring of a PEM electrolyser based on dynamical modelling,” *Int. J. Hydrogen Energy*, vol. 34, no. 14, pp. 5992–5999, 2009

[5] M. W. Bernardi, Dawn M., Verbrugge, “Mathematical model of a gas diffusion electrode bonded to a polymer electrolyte,” *AIChE J.*, vol. 37, no. 8, pp. 1151–1163, 1990

[6] H. Görgün, “Dynamic modelling of a proton exchange membrane (PEM) electrolyzer,” *Int. J. Hydrogen Energy*, vol. 31, no. 1, pp. 29–38, 2006.

[7] R. W. Kopitzke, C. A. Linkous, H. R. Anderson, and G. L. Nelson, “Conductivity and Water Uptake of Aromatic-Based Proton Exchange Membrane Electrolytes,” J. Electrochem. Soc., vol. 147, no. 5, pp. 1677–1681, 2000

[8] T. E. Springer, T. a. Zawodzinski, and S. Gottesfeld, “Polymer electrolyte fuel cell model,” *J. Electrochem. Soc.*, vol. 138, no. 8, pp. 2334–2342, 1991

[9] P. Medina and M. Santarelli, “Analysis of water transport in a high pressure PEM electrolyzer,” *Int. J. Hydrogen Energy*, vol. 35, no. 11, pp. 5173–5186, 2010

[10] S. Dutta, S. Shimpalee, and J. W. Van Zee, “Numerical prediction of mass-exchange between cathode and anode channels in a PEM fuel cell,” *Int. J. Heat Mass Transf.*, vol. 44, no. 11, pp. 2029–2042, 2001

[11] G. Lin *et al.*, “Modeling Liquid Water Effects in the Gas Diffusion and Catalyst Layers of the Cathode of a PEM Fuel Cell service,” *J. Electrochem. Soc.*, vol. 151, no. 12, pp. A1999–A2006, 2004

[12] F. Marangio, M. Santarelli, and M. Calì, “Theoretical model and experimental analysis of a high pressure PEM water electrolyser for hydrogen production,” *Int. J. Hydrogen Energy*, vol. 34, no. 3, pp. 1143–1158, 2009

[13] S. A. Grigoriev, P. Millet, S. A. Volobuev, and V. N. Fateev, “Optimization of porous current collectors for PEM water electrolysers,” *Int. J. Hydrogen Energy*, vol. 34, no. 11, pp. 4968–4973, 2009

[14] M. Santarelli, P. Medina, and M. Calì, “Fitting regression model and experimental validation for a high-pressure PEM electrolyzer,” *Int. J. Hydrogen Energy*, vol. 34, no. 6, pp. 2519–2530, 2009